to appear in the book *The Physics of Multiply and Highly Charged Ions*
(ed. R. W. McCullough and F. J. Currell, Kluwer Academic, London, 2002)

COLLISION PHENOMENA INVOLVING HIGHLY-CHARGED IONS IN ASTRONOMICAL OBJECTS

A. Chutjian
Jet Propulsion Laboratory, California Institute of Technology
Pasadena, CA 91109 USA
(revised 7/5/01)

I Introduction

This decade has seen a dramatic and international growth in space observations from an impressive array of ground and space-borne instruments. These efforts have been led by the U.S. National Aeronautics and Space Administration and the European Space Agency. The observational platforms include the Infrared Space Observatory, the Hubble Space Telescope, the Extreme Ultraviolet Explorer (*EUVE*), *SOHO*, the Roentgen Satellite *(ROSAT)*, the Far Ultraviolet Spectroscopic Explorer (*FUSE*), *Chandra*, XMM-*Newton*, *TRACE*; as well as upcoming missions such as *SOFIA*, Space Infrared Telescope Facility (*SIRTF)* and Constellation-X. Each platform has one or more spectrometers covering a range of wavelengths, from the infrared (*ISO*) to the X-ray regions (XMM-*Newton, Chandra*, Constellation-X). These spectrometers are *remote sensing*, as opposed to *in-situ* instruments which measure neutrals and charged particles from the Sun, a planet, or in the interstellar medium using neutral imagers, ion analyzers, electron analyzers, and mass spectrometers. As such, the business of these instruments is detection of photons, either through imaging instruments or spectrometers. One can obtain, for example, *images* of the Sun in the Fe IX $^1P^o \rightarrow {}^1S$ λ171 Å, Fe XII $^4P \rightarrow {}^4S^o$ λ195 Å, Fe XV $^1P^o \rightarrow {}^1S$ λ284 Å, and He II $^2P^o \rightarrow {}^2S$ λ304 Å emission lines using the Extreme Ultraviolet Imaging Telescope (*EIT*) aboard *SOHO* [1]. One can also obtain *spectra* of the astronomical object, such as those returned by the *SUMER/SOHO* high-resolution spherical concave grating instrument [2]. Imaging information is useful for monitoring the morphology of the object, such as changes in the solar coronal and transition region due to coronal loops and

mass ejections. Spectral data are critical for obtaining ionic species, densities, and electron temperatures from stars, the Sun, active galactic nebulae (AGNs), *etc.*[3]

In the following summaries the role of highly charged ions (HCIs) in the various astronomical objects will be summarized. Included will be the use of critical quantities such as cross sections for excitation, charge-exchange, X-ray emission, radiative recombination (RR) and dielectronic recombination (DR); and lifetimes, branching ratios, and A-values. These data, experimental and calculated, are required for interpretation of the spectral observations [4]. The astronomical objects include the Sun and stars, circumstellar clouds, the interstellar medium, planetary ionospheres, planetary magnetospheres (*e.g.*, the Io-Jupiter torus), and comets. The processes and their interpretation parallel in many respects the phenomena occurring in confined fusion plasmas where stellar-like temperatures are achieved. Unfortunately, space does not permit a treatment of these plasmas. The approaches summarized in Refs. [5-8] afford an entry into this parallel universe of the tokamak, JET, ITER, the National Ignition Facility, and the LaserMegajoule.

II Basic Collision Phenomena and Atomic-Physics Parameters

A Electron Excitation and Recombination in the HCIs

The spectrally-resolved photon emissions from the hot solar or stellar plasma are analyzed in terms of spectral line ratios to obtain the plasma properties. With increasing resolution of the spacecraft spectrometers, from the infrared to X-ray spectral regions, many once-blended emission lines can now be resolved, and hence many more useful line intensities and ratios are being established.

One of the most basic and important phenomena occurring in the high electron-temperature plasmas is the electron-impact (collisional) excitation of emitting spectral lines in the HCI. Electron temperatures and densities may be deduced from the line intensity ratios through the standard expressions for the statistical equilibrium. One treats the rate of change of the population of the emitting upper (i or j) state to the ground (g) state, taking into account all

other levels. This process involves a large range of atomic data, such as level lifetimes and excitation cross sections (collision strengths).

For a simple three-level case the ratio of line intensities is given by [9,10],

$$\frac{I(i \to g)}{I(k \to g)} = \frac{C(g \to i)}{C(g \to k)} \left(1 + \frac{N_e C(k \to m)}{A(k \to g)} \right). \qquad (1)$$

Here, the C's are thermally-averaged collision strengths for which standard expressions are given [11], and $A(k \to g)$ is the Einstein A-coefficient for spontaneous radiation in the $k \to g$ transition. For small collision strengths $C(k \to m)$, low electron density N_e, and for an optically-allowed transition one has $A(k \to g) >> N_e\, C(k \to m)$, so that the line ratio is density insensitive, but may be T_e-sensitive *via* the behavior of the collision-strength ratio in Eq. [1]. This is the so-called coronal equilibrium limit. To qualify as useful diagnostics, the candidate line ratios should be monotonically increasing or decreasing in the range of desired plasma electron temperature T_e or electron density N_e. Otherwise, if a particular ratio is flat, then the astrophysical measurement of the ratio can lead to a wide and not helpful range for T_e or N_e. Many examples exist of the use of ratios, and recent calculations have been published for Fe XXI [12], Ca XVI [13], and Si VIII, S X [14]. By way of example, shown in Fig. 1 are two calculated line ratios R_1 and R_2 as a function of N_e in Fe XXI. These ratios are given by,

$$R_1 = I(2s^2 2p^2\ {}^3P_1 - 2s2p^3\ {}^5S) \,/\, I(2s^2 2p^2\ {}^3P_0 - 2s^2 2p^2\ {}^3P_1), \text{ and}$$
$$R_2 = I(2s^2 2p^2\ {}^3P_1 - 2s^2 2p^2\ {}^1S) \,/\, I(2s^2 2p^2\ {}^3P_0 - 2s^2 2p^2\ {}^3P_1).$$

One sees from Fig. 1 that the ratio is a relatively flat function of N_e at $N_e \leq 10^{11}$ cm^{-3}, hence there is no accurate measure of electron density at any T_e. Above 10^{11} cm^{-3} one can, from knowledge of the measured ratio, pick off values of N_e and T_e using the family of calculated curves. As noted in Ref. [12], the ratios are useful in analyzing the plasma arising from an energetic solar or stellar flare; and emission from Fe impurities in a fusion plasma. The data of Fig. 1 are all calculated results. There are at the moment no experimental data to provide a cross check of the level of theoretical approximations.

The use of Eq. [1] requires knowledge of not only excitation cross sections *via* the C's, but also of level lifetimes and branching ratios to obtain the A's. Since excitation can occur from the kth level (which may be metastable) to all other levels m, a wide range of collision strengths is required, covering a multitude of transitions. Moreover, a respectable degree of accuracy in the atomic parameters is needed, almost always to better than 10%. As pointed out by Malinovsky *et al.* [16], shortcomings in the calculation of cross sections or A-values can detract from the usefulness of a line ratio. Hence the calculations, carried out in an appropriate theory, should address the following: the required size of the configuration-interaction expansion; resonances at the excitation threshold, especially for spin- and symmetry-forbidden transitions; a proper wavefunction description of the target to give the spectroscopic energy levels and oscillator strengths (length and velocity); use of continuum orbitals to describe short-range electron correlations and pseudostates to describe resonances; sufficient number of partial waves; relativistic effects, *etc.* By the same token, experimental measurements of absolute excitation cross sections in HCIs must access both spin- and symmetry-allowed and -forbidden transitions; be able to access the threshold region, with extension to higher energies; account for metastable levels in the target beam current; and be free of (or corrected for) electron-ion elastic scattering. Moreover, when optical-emission and detection methods are used, the cross sections become *effective* excitation cross sections, as cascading contributions from excited electronic states will contribute to the measured emission.

The electron energy-loss approach, in both crossed beams [17-20] and merged beams [21-24] geometries affords many of the experimental advantages. In addition, those measurements are free of cascading contributions, since only a single energy-loss electron can result from excitation of the upper state. Finally, the merged-beams geometry allows one to measure the integral excitation cross section directly, rather than an angle-by-angle differential cross section, which is then integrated. Angular differential measurements provide a more critical test of physics theory, whereas only integral cross sections (at least at the moment) are used in the astrophysics models.

Comparisons of theory and experiment are steadily being published. The results to date show that the multistate $\boldsymbol{R}$-matrix approach to the calculation of HCI excitation cross sections in

the threshold region generally agrees with experiment, to within the combined uncertainties. Such comparisons have been made for transitions in the HCI systems e-C^{3+} [25], e-O^{2+} [26], e-O^{5+} [21, 27], e-Si^{2+} [28], e-Si^{3+} [23], e-S^{2+} [29], e-Ar^{6+} [30], and e-Ar^{7+} [31]. In both e-O^{2+} and e-S^{2+} experiment and theory were able to account for the rich resonance structure at threshold. An example of the resonance structure in e-S^{2+} excitation is shown in Fig. 2 for the spin-forbidden $3s^23p^2\ ^3P \rightarrow 3s3p^3\ ^5S^o$ transition. The experimental resolution was 80 meV in the center-of-mass frame, sufficient in many cases to resolve the multitude of overlapping, narrow resonances. Excitation rates for charge states of O and S are needed to understand the T_e, N_e, and energy balance in the Io-Jupiter plasma torus [32-34]. Long path length absorption by O^{5+} is commonly seen in our own Milky Way gas [35]. Emission lines in O^{5+} and S^{5+}, as well as lines in C^{2+}, Ne^{4+}, and Ne^{5+}, have been detected in supernova remnant N49 by the *FUSE* satellite [36]. Higher charge states such as Si^{13+}, S^{15+}, and Fe^{24+} are seen by XMM-*Newton* at the cataclysmic variable *OY Car* [37], and Mg^{11+}, Ca^{18+}, and Ar^{16+} have been recorded by *Chandra* at *Capella* and at the binary HR 1099 [38].

Another important plasma property is the ionization fraction for each species; *i.e.*, the fraction of ions in a particular charge state as a function of solar/stellar temperature. These calculations require a large set of electron ionization and recombination cross sections for both direct and indirect processes (such as inner-shell excitation followed by autoionization). For example, high charge states of iron are common to the sun and stars. Charge states up to Fe^{25+} are seen in the more violent events, such as solar flares as observed by the Bragg Crystal Spectrometer (BCS) aboard the Japanese *Yohkoh* satellite, and in the *Chandra* X-ray observations of the Seyfert galaxy *Markarian 3* [39]. In the BCS measurements, the flare temperature could be derived from the intensity ratio of a line formed by dielectronic capture to Fe XXV, relative to the intensity of a collisionally-excited resonance line in Fe XXV [40]. For general plasma modeling, a complete data set of ionization cross sections was used in a calculation of ionization and recombination rates as a function of T_e in plasmas containing charge states Fe^{14+} to Fe^{25+} [41]. The accurate measurement [42] and calculation [43] of ionization cross sections in HCIs not only reveal the physics of ionization but also provide important inputs to the ionization models.

Accurate DR cross sections are needed to establish diagnostic intensity ratios. It is well known that plasma microfields **E** of less than about 100 V/m, and motional electric fields can have a large effect on both the RR [44] and the DR cross sections [45-48]. Electric fields of the order of 100 V m^{-1} are sufficient to change DR rates by factors of 3-5 through mixing of ℓ levels [47-49]. Moreover, DR rate enhancements of up to 2 have been detected for Ti^{19+} in crossed **E**×**B** fields, with **B** in the range 30-80 mT [46]. This effect arises through the fact that the magnetic quantum number m is no longer a good quantum number in the crossed-fields geometry, and influences the ℓ mixing brought on by **E**. Our Sun's magnetic fields range from about 1 mT in the coronal region to 500 mT at the center of a sunspot umbra [50]. Hence *both* **E** (Stark) and **B** (Zeeman) mixing can effect DR rates in the Sun and stars. It is clear that as observations become more spatially localized, and the plasma models more sophisticated, one will have to take into account field effects on the cross sections in localized regions of high **E** and **B**.

The need in astrophysics for accurate data on all iron charge states is considerable. The IRON project is dedicated to the calculation of collision strengths, photoionization cross sections, oscillator strengths, radiative and DR cross sections in mainly Fe ions [51]. Because of the inherent difficulty of generating high Fe charge states in the laboratory practically all the plasma parameters are calculated quantities, with almost no comparisons to experiment. The ion storage ring TSR in Heidelberg has been used to measure DR rate coefficients in Fe XVIII and Fe XIX [52]. Line emission in the 10.5-11.5 Å wavelength range corresponding to direct, resonant, and dielectronic excitations in the e-Fe XXIV system has been reported using the electron beam ion trap (EBIT) at Lawrence Livermore National Laboratory [53]. There is good agreement with distorted-wave and ***R***-matrix calculations. Data on collisional excitation of *any* Fe charge state is non-existent. As one part of a larger program involving Fe and Mg charge states, excitation cross sections have been reported for the $3s^2 3p^5\ ^2P^o_{3/2} \rightarrow 3s^2 3p^5\ ^2P^o_{1/2}$ λ6376 Å coronal red line in Fe^{9+} using the JPL electron cyclotron resonance ion source [54].

In order to make data available to modelers, experimentalists and theoreticians, the experimental and theoretical data are submitted to central databases. One frequently-used center is the *CHIANTI* atomic database [55].

B Optical Absorption and Emission in the HCIs

Elemental abundances in the interstellar medium (ISM) are obtained through measurement of absorption intensities (equivalent widths) at the atomic and molecular wavelengths, using a bright star as the background continuum source. For example, recent Goddard High Resolution Spectrograph observations from the Hubble Space Telescope (GHRS/HST) reveal absorptions due to Si^{3+}, $C^{3+,}$ N^{4+}, and O^{5+} towards the Seyfert galaxy ESO 141-055 [56]. The wavelength range here is $\lambda\lambda$ 1030-1550 Å. An example of the use of the *CHIANTI* database in conjunction with a stellar superoutburst is shown in Fig. 3 [57]. Rich emissions in O^{5+}, $Ne^{5,6+}$, Si^{4+}, and $Fe^{8,9+}$ are evident.

Emissions in HCIs are also detected by observation of solar/stellar winds, and of our own Sun. *FUSE* has recorded emissions from stellar winds emanating from two supergiants in the Small Magellanic Cloud (SMC) and the LMC [58]. Emissions in C^{2+}, $N^{3+,}$ O^{5+}, S^{3+}, S^{5+}, and P^{4+} are detected. Because of the greater sensitivity of *FUSE*, one is able to detect weaker absorptions and emissions. Hence absorption lines will tend to be unsaturated. Weak features will lie on the linear part of the curve of growth, leading to reliable measurements *via* the less-abundant elements or *via* optically-forbidden absorptions.

Column densities, or the integrated intensity of absorption along the line of sight between object and spectrometer, may be obtained from the expression for the so-called equivalent width of the absorption line given by [59],

$$W_\lambda = \int \left[1 - \frac{I_\nu}{I_\nu(0)} \right] d\lambda \,. \tag{2}$$

W_λ is the integrated area (in cm) at the wavelength λ (frequency ν) absorbed out of a background continuum by the absorbing species. The quantity I_ν (0) is the transmitted intensity in the absence of the line, and W_λ is related to the particle density by (in *cgs* units),

$$\frac{W_\lambda}{\lambda} = \frac{\pi e^2}{m_e c^2} N_j \lambda f_{jk} \ , \qquad (3)$$

where e is the electron charge, m_e the electron mass, c the speed of light, and f_{jk} the absorption oscillator strength for transition between lower level j and upper level k. The quantity N_j is the number of absorbing molecules/cm^2 which is the desired elemental abundance in that region of the interstellar medium (ISM).

Use of Eq. (3) requires f_{jk} for the relevant transition in the neutral or ionized species along the line-of-sight. Since the accuracy of N_j is directly proportional to that of the f_{jk}, one would like oscillator strengths accurate to better than 10%. As is the case with collision strengths, experiment can only provide a handful of measured oscillator strengths for some HCIs and some transitions. The remaining have to be calculated through benchmarked theoretical methods. Many accurate measurements of lifetimes in HCIs are obtained in ion storage rings [60], the EBIT [61], and the Kingdon ion trap [62]. Representative examples are lifetimes for N^{5+} [63], Be-like N^{3+} and O^{4+} [64], intermediate-Z, He-like ions [65], and lifetimes for the coronal transitions in Fe^{9+} and Fe^{13+} [66].

Results of recent calculations of level lifetimes and oscillator strengths may be found in representative publications using the Breit-Pauli Hamiltonian in the *CIV3* atomic structure code, and the ***R***-matrix method [67-73]. The order of 10^4 radiative transitions can be required to model stellar atmospheres and stellar spectra [74]!

Both the need for atomic A-values and collisions strengths in astrophysical observations, and the power of present-day orbiting X-ray spectrometers is best illustrated by recent data from *Chandra's* Low-Energy Transmission Grating Spectrometer (LETGS) [75] and XMM-*Newton's* Reflection Grating Spectrometer (RGS) [76]. The LETGS is a diffraction grating spectrometer with a resolution of ≈0.06 Å over the wavelength range 2-175 Å (0.07-6 keV). Shown in Fig. 4 is the LETGS X-ray spectrum at the star *Capella* of the He-like triplets in C V, N VI, and O VII. These are the so-called forbidden (f) 1s2s ^{3}S → 1s^2 ^{1}S, intersystem (i) (1s2p ^{3}P^o + 1s2s ^{1}S) → 1s^2 ^{1}S, and resonance (r) 1s2p ^{1}P^o → 1s^2 ^{1}S transitions. The observed intensity ratios f/i and $(f + i)/r$ are used as density diagnostics. Due to the absence of experimental data the collision strengths

for these ratios (needed to back out the electron density) were calculated ones in an early distorted-wave theory [77].

C Highly-Charged Ions in Solar and Stellar Winds

Exciting and unexpected interactions of HCIs with neutrals were detected *via* resulting X-rays detected at the comet C/Hyakutake 1996 B2 [78] using *ROSAT*; and most recently of comet C/Linear 1999 S4 using the *Chandra* X-ray Observatory [79]. X-ray observations have also been reported from EUVE for the comets d'Arrest, Borrelly, Bradfield, Encke, Hyakutake, Hale-Bopp, and Mueller [80-84]. Further studies of the X-rays from Hale-Bopp [80-82] and Levy, Tsuchiya-Kiuchi, Honda-Mrkos-Pajdušáková and Arai [85] have also been reported.

It appears that X-ray emission from comets is definitely a general phenomenon. Furthermore, the phenomena would appear to extend to *other* astrophysical objects where any "wind" of highly-charged ions (HCIs) can scatter from a neutral cloud, whether the cloud be from a comet, a planetary atmosphere [86], or a circumstellar neutral cloud or the ISM impinged by a stellar wind [87]. Predictions have been made of X-rays emitting by charge-transfer collisions of heavy solar-wind HCIs and interstellar/interplanetary neutral clouds [88].

As to the origin of the comet X-rays, it was initially suggested that the emissions could be explained by bremsstrahlung associated with hot electrons in the solar wind interacting with the cometary plasma [89]. These and other mechanisms, such as scattering of solar X-rays, and the interaction of the HCIs with cometary dust particles, were studied [80,90] and some mechanisms were rejected. The two mechanisms currently in favor are: (a) production of X-rays from charge-exchange with the cometary neutral gases, and (b) bremsstrahlung between the solar-wind electrons and the cometary neutrals [89]. The charge-exchange mechanism successfully accounts for the X-ray spectral energies and intensities based on best knowledge of ion fluxes and neutral densities [79-83,85,90-95]. In this scenario highly-stripped solar-wind ions interact with the cometary neutral species. The excited, recombined solar-wind HCIs emits X-rays as they cascade to their ground electronic states. A list of the HCI abundances used in recent modeling [95] is given in Table 1.

Using O^{8+} as an example of a solar-wind ion, and neutral H_2O as a cometary species, the overall mechanism is,

$$O^{8+} + H_2O \rightarrow O^{7+*} + H_2O^{+} , \tag{4}$$

where the excited O^{7+*} ions emit X-ray photons. Detailed X-ray spectra and absolute charge-exchange cross sections are required for modeling the spectra and intensity in the *ROSAT*, EUVE, *Chandra*, and XMM-*Newton* observations. Using contributions from the many solar wind species and charge states, the expected fluctuation of X-ray intensity have been calculated [94] as a function of fast (750 km/s) and slow (400 km/s) solar winds, and optically thick and thin scattering [95]. One result of Ref. [95] is shown in Fig. 5. In the absence of data assumptions had to be made about (a) the energy dependence of the single charge exchange cross sections (assumed flat with ion energy), and about the magnitude of the multiple charge exchange cross sections (neglected). The charge-exchange cross sections were calculated [96] from the expression given by the over-barrier model [97],

$$n \leq q\left(2I_p\left(1+\frac{q-1}{2\sqrt{q}+1}\right)\right)^{-1/2} , \tag{5}$$

where n is the largest integer satisfying the inequality, q is the ionic charge and I_p is the ionization potential (au). The charge-exchange cross sections $\sigma_{q\,q'}$ between ionic states q and q' are given as $\sigma_{q\,q'} = 0.88 \times 10^{-16}\ R_c^2\ cm^2$, where the crossing radius R_c is given as,

$$R_c = \frac{q-1}{q^2/2n^2 - I_p} . \tag{6}$$

Where comparisons can be made between actual measurements and Eq. (6), factors-of-two differences exist. For example, the single-exchange cross sections <u>*assumed*</u> [81] *vs* <u>*measured*</u> [98] for $O^{5+} + H_2O$ collisions are (in units of 10^{-15} cm^2) 2 *vs* 4.3; and for $O^{7+} + H_2O$, 12 *vs* 5.3. Accurate single and multiple charge-exchange cross sections [99] and X-ray emission cross sections must be measured for the various ionization states of the solar-wind species C, N, O, Ne, Mg, Si, Fe in the relevant solar-wind velocity range, and in collisions with neutral cometary species (Table 1).

Shortly after the first ROSAT X-ray observations were reported, laboratory measurements were started on X-ray emission spectra for collisions of some of the partially- and fully-stripped ions in Table 1 interacting with the major comet gases. These gases were CO, CO_2, and H_2O (and will also include NH_3). X-ray spectra for the system of fully-stripped oxygen $O^{8+} + H_2O$ [Eq. (4)] and $O^{8+} + CO_2$ are shown in Fig. 6. X-ray emission cross sections were obtained from these spectra by fitting the peaks to the underlying Lyman transitions $np \rightarrow 1s$ for the H-like O^{7+} ion, then normalizing the area to the total charge-exchange cross section, and correcting for cascades which populate metastable levels that decay outside the field-of-view of the detector [98].

One sees that the data of Fig. 6 are a subset of the total emission channels addressed in Fig. 5. There is a continuing need for emission cross sections for the system parameters listed in Table 1, with attention to relevant species in the comet, planetary atmosphere [86], the ISM [87,88], *etc.* Moreover, the energy range of required data is not limited to that in Table 1, but can extend to several MeV/amu for charge transfer collisions with H_2 in the Jovian magnetosphere [86].

III Summary

Laboratory collision physics involving highly-charged ions has direct contact with astrophysical phenomena. The surprising observation of cometary X-rays was quickly addressed both theoretically and (thanks to earlier investments in laboratory infrastructure by funding agencies) by laboratory measurements. A full range of atomic collision data is required to obtain accurate photon-emission intensities. These intensities can then be related back to electron and ion temperatures, densities, and ionization fractions in the astronomical plasma. A large body of data is needed for many phenomena; and for combinations of many transitions in a variety of ions and their charge states. Almost certainly the lion's share of the data must be calculated within an accurate theory. Experiment must be used to provide missing data and be required to provide critical tests of theory, as "ground truth." Those benchmarked theories can then, with higher confidence, be used to calculate collision phenomena for ions/charge-states/transitions where comparisons have not been made, usually for reasons of time and resolution.

In summary, the required data and their application are:

(a) collision strengths for obtaining collisional excitation rates, assuming usually a Maxwellian electron energy distribution function in the astrophysical plasma,
(b) lifetimes, branching ratios, and Einstein A-values for the coronal models,
(c) direct ionization and indirect ionization cross sections, for both outer- and inner-shell electrons, to calculate ionization fractions in the plasma,
(d) radiative and dielectronic recombination cross sections for calculation of ionization fractions,
(e) dependencies of cross sections and lifetimes on ℓ, m level mixing by external **E** and **B** fields, such as encountered in a stellar object and within sunspots or high-velocity explosive events,
(f) single and multiple charge-exchange cross sections from about $1\text{-}10^5$ keV/amu for understanding solar- and stellar-wind interactions with comets and circumstellar neutral clouds ; and for neutral collisions with magnetospherically-accelerated ions,
(g) X-ray emission cross sections in (f), with the relevant neutral atomic or molecular target.

There are other no less-important atomic parameters which go into a complete model. These include accurate HCI energy levels (wavelengths), damping constants for atomic lines, photoionization cross sections, isotopic splittings, and hyperfine splittings. It is clear that space-based and ground-based instruments are becoming more sophisticated, sensitive, and able to cover a wider wavelength range at resolutions and sensitivities that are even challenging to laboratory instruments (*e.g.*, the GHRS and STIS spectrometers on *HST*). With increasing resolution, for example, more spectral lines can be identified, resulting in a wider range of detected species requiring more of (a)-(g) above. This trend will clearly continue with SOFIA and Constellation-X.

This work was carried out at the Jet Propulsion Laboratory/California Institute of Technology, and was supported under contract with the National Aeronautics and Space Administration.

References

[1] D. Moses and 34 co-authors, *Solar Physics 175*, 571 (1997); U. Feldman, I. E. Dammasch, and K. Wilhelm, *Space Science Revs. 93,* 411 (2000).

[2] K. Stucki, S. K. Solanki, U. Schühle, I. Rüedi, K. Wilhelm, J. O. Stenflo, A. Brković, and M. C. E. Huber, *Astronom. Astrophys. 363*, 1145 (2000).

[3] U. Feldman, W. Curdt, E. Landi, and K. Wilhelm, *Astrophys. J. 544,* 508 (2000).

[4] See the issue, "Electron Excitation Data for Analysis of Spectral Line Radiation from Infrared to X-Ray Wavelengths: Reviews and Recommendations," *Atom. Data Nucl. Data Tables 57* (1994).

[5] See, for example, *Atomic and Molecular Processes in Fusion Edge Plasmas* (Plenum, NY, 1995).

[6] I. H. Coffey, R. Barnsley, F. P. Keenan, and N. J. Peacock, *J. Phys. B 27*, 1011 (1994).

[7] S. H. Glenzer and 12 co-authors, *Phys. Plasmas 6*, 2117 (1999).

[8] R. A. Phaneuf, *Physica Scripta T47,* 124 (1993).

[9] A. H. Gabriel and C. Jordan, in *Case Studies in Atomic Collision Physics II* (ed. E. W. McDaniel and M. R. C. McDowell, American Elsevier, NY 1972), Ch. 4.

[10] A. H. Gabriel and H. E. Mason, in *Applied Atomic Collision Physics* (eds. H. Massey, E. W. McDaniel, and B. Bederson, Academic, NY 1982), Vol. 1, Ch. 10.

[11] S. S. Tayal, A. K. Pradhan, and M. S. Pindzola, in *Atomic and Molecular Processes in Fusion Edge Plasmas* (Plenum, NY, 1995) Ch. 6.

[12] F. P. Keenan, V. J. Foster, K. M. Aggarwal, and K. G. Widing, *Solar Physics 169*, 47 (1996).

[13] F. P. Keenan, D. J. Pinfield, V. J. Woods, R. H. G. Reid, E. S. Conlon, A. K. Pradhan, H. L. Zhang, and K. G. Widing, *Astrophys. J. 503*, 953 (1998).

[14] G. A. Doschek, H. P. Warren, J. M. Laming, J. T. Mariska, K. Wilhelm, P. Lemaire, U. Schühle, and T. G. Moran, *Astrophys. J. 482,* L109 (1997).

[15] H. E. Mason, G. A. Doschek, U. Feldman, and A. K. Bhatia, *Astron. Astrophys. 73*, 74 (1979).

[16] M. Malinovsky, *Astron. Astrophys. 43*, 101 (1975); M. Malinovsky, L. Heroux, and S. Sahal-Bréchot, *Astron. Astrophys. 23,* 391 (1973).

[17] A. Chutjian and W. R. Newell, *Phys. Rev. A 26*, 2271 (1982).

[18] I. D. Williams, A. Chutjian and R. J. Mawhorter, *J. Phys. B 19*, 2189 (1986).

[19] B. A. Huber, C. Ristori, C. Guet, D. Küchler, and W. R. Johnson, *Phys. Rev. Lett. 73*, 2301 (1994).

[20] I. D. Williams, B. Srigengan, A. Platzer, J. B. Greenwood, W. R. Newell, and L. O'Hagan, *Phys. Scripta T73*, 121 (1997).

[21] J. A. Lozano, M. Niimura, S. J. Smith, A. Chutjian, and S. S. Tayal, *Phys. Rev. A 63,* 042713 (2001).

[22] S. J. Smith, K.-F. Man, R. J. Mawhorter, I. D. Williams and A. Chutjian, *Phys. Rev. Letters 67*, 30 (1991).

[23] E. K. Wåhlin, J. S. Thompson, G. H. Dunn, R. A. Phaneuf, D. C. Gregory, and A. C. H. Smith, *Phys. Rev. Lett. 66*, 157 (1991).

[24] O. Woitke, N. Djurić, G. H. Dunn, M. E. Bannister, A. C. H. Smith, B. Wallbank, N. R. Badnell, and M. S. Pindzola, *Phys. Rev. A 58*, 4512 (1998).

[25] J. B. Greenwood, S. J. Smith, A. Chutjian, and E. Pollack, *Phys. Rev. A 59,* 1348 (1999).

[26] M. Niimura, S. J. Smith, and A. Chutjian, *Astrophys. J.* (in press).

[27] E. W. Bell and 15 co-authors, *Phys. Rev. A 49*, 4585 (1994).

[28] B. Wallbank, N. Djurić, O. Woitke, S. Zhou, G. H. Dunn, A. C. H. Smith, and M. E. Bannister, *Phys. Rev. A 56,* 3714 (1997).

[29] S. J. Smith, J. B. Greenwood, A. Chutjian, and S. S. Tayal, *Astrophys. J. 541*, 501 (2000).

[30] Y-S. Chung, N. Djurić, B. Wallbank, G. H. Dunn, M. E. Bannister, A. C. H. Smith, *Phys. Rev. A 55*, 2044 (1997).

[31] X. Q. Guo, E. W. Bell, J. S. Thompson, G. H. Dunn, M. E. Bannister, R. A. Phaneuf, and A. C. H. Smith, *Phys. Rev. A 47*, R9 (1993).

[32] F. Herbert and D. T. Hall, J. *Geophys. Res. 103*, 19 915 (1998).

[33] D. T. Hall, G. R. Gladstone, H. W. Moos, F. Bagnal, J. T. Clarke, P. D. Feldman, M. A. McGrath, N. M. Schneider, D. E. Shemansky, D. F. Strobel, and J. H. Waite, *Astrophys. J. Lett. 426,* L51 (1994).

[34] D. E. Shemansky, *J. Geophys. Res. 93*, 1773 (1988).

[35] B. D. Savage, K. R. Sembach, E. B. Jenkins, J. M. Shull, D. G. York, G. Sonneborn, H. W. Moos, S. D. Friedman, J. C. Green, W. R. Oegerle, W. P. Blair, J. W. Kruk, and E. M. Murphy, *Astrophys. J. Lett.* 538, L27 (2000).

[36] W. P. Blair, R. Sankrit, R. Shelton, K. R. Sembach, H. W. Moos, J. C. Raymond, D. G. York, P. D. Feldman, P. Chayer, E. M. Murphy, D. J. Sahnow, and E. Wilkinson, *Astrophys. J. Lett. 538*, L61 (2000).

[37] G. Ramsay, F. Córdova, J. Cottam, K. Mason, R. Much, J. Osborne, D. Pandel, T. Poole, and P. Wheatley, *Astron. Astrophys. 365*, L294 (2001).

[38] T. R. Ayres, A. Brown, R. A. Osten, D. P. Huenemoerder, J. J. Drake, N. S. Brickhouse, and J. L. Linsky, *Astrophys. J. 549,* 554 (2001).

[39] M. Sako, S. M. Kahn, F. Paerels, and D. A. Liedahl, *Astrophys. J. Lett. 543*, L115 (2000).

[40] G. A. Doschek, *Astrophys. J. 527*, 426 (1999); G. A. Doschek and U. Feldman, A*strophys. J. 313*, 883 (1987).

[41] M. Arnaud and J. Raymond, *Astrophys. J. 398,* 394 (1992).

[42] R. Rejoub and R. A. Phaneuf, *Phys. Rev. A 61*, 032706 (2000).

[43] J. Colgan, D. M. Mitnick, and M. S. Pindzola, *Phys. Rev. A 63*, 012712 (2000).

[44] G. Gwinner and 16 co-authors, *Phys. Rev. Letters 84*, 4822 (2000).

[45] T. Bartsch, S. Schippers, A. Müller, C. Brandau, G. Gwinner, A. A. Saghiri, M. Beutelspacher, M. Grieser, D. Schwalm, A. Wolf, H. Danared, and G. H. Dunn, *Phys. Rev. Lett. 82*, 3779 (1999).

[46] T. Bartsch, S. Schippers, M. Beutelspacher, S. Böhm, M. Grieser, G. Gwinner, A. A. Saghiri, G. Saathoff, R. Schuch, D. Schwalm, A. Wolf, and A. Müller, *J. Phys. B. 33*, L453 (2000).

[47] A. R. Young, L. D. Gardner, D. W. Savin, G. P. Lafyatis, A. Chutjian, S. Bliman, and J. L. Kohl, *Phys. Rev. A 49*, 3577 (1994); D. W. Savin, L. D. Gardner, D. B. Reisenfeld, A. R. Young, and J. L. Kohl, *Phys. Rev. A 53*, 280 (1996).

[48] D. B. Reisenfeld, J. C. Raymond, A. R. Young, and J. L. Kohl, *Astrophys. J. Lett. 389*, L37 (1992); D. B. Reisenfeld, *Astrophys. J. 398*, 386 (1992).

[49] T. Bartsch and 12 co-authors, *Phys. Rev. Letters, 79,* 2244 (1997).

[50] K. J. H. Phillips, *Guide to the Sun* (Cambridge, 1992).

[51] M. C. Chidichimo, V. Zeman, J. A. Tully, and K. A. Berrington, *Astron. Astrophys. Suppl. Ser. 137*, 175 (1999); K. Butler, *Phys. Scripta T65,* 63 (1996).

[52] D. W. Savin and 15 co-authors, *Astrophys. J. Suppl. Ser. 123,* 687 (1999).

[53] M. F. Gu, S. M. Kahn, D. W. Savin, P. Beiersdorfer, G. V. Brown, D. A. Liedahl, K. J. Reed, C. P. Bhalla, and S. R. Grabbe, *Astrophys. J. 518,* 1002 (1999).

[54] M. Niimura, S. J. Smith, I. Ćadež, and A. Chutjian, *XXII Int. Conf. Photonic Electronic Collisions* (Santa Fe, NM, 7/01).

[55] E. Landi, M. Landini, K. P. Dere, P. R. Young, and H. E. Mason, *Astron Astrophys. 135,* 339 (1999).

[56] K. R. Sembach, B. D. Savage, and M. Hurwitz, *Astrophys. J. 524,* 98 (1999).

[57] C. W. Mauche and J. C. Raymond, Astrophys. J. 541, 24 (2000).

[58] A. W. Fullerton and 12 co-authors, *Astrophys. J. Lett. 538,* L46 (2000).

[59] L. Spitzer, *Physical Process in the Interstellar Medium* (Wiley, New York, 1978) Ch. 3; B. D. Savage and K. R. Sembach, *Astrophys. J. 379,* 245 (1991).

[60] E. Träbert, A. G. Calamai, J. D. Gillaspy, G. Gwinner, X. Tordoir, and A. Wolf, *Phys. Rev. A 62,* 022507 (2000).

[61] E. Träbert, P. Beiersdorfer, S. B. Utter, G. V. Brown, H. Chen, C. L. Harris, P. A. Neill, D. W. Savin, and A. J. Smith, *Astrophys. J. 541,* 506 (2000); E. Träbert, *Phys. Scripta 61,* 257 (2000).

[62] D. A. Church, *Phys. Rep. 228,* 253 (1993); D. A. Church, D. P. Moehs, and M. Idrees Bhatti, *Int. J. Mass Spectrom. 192,* 149 (1999); D. P. Moehs, D. A. Church, M. I. Bhatti, and W. F. Perger, *Phys. Rev. Lett. 85,* 38 (2000).

[63] P. A. Neill, E. E. Träbert, P. Beiersdorfer, G. V. Brown, C. L. Harris, S. B. Utter, and K. L. Wong, *Phys. Scripta, 62,* 141 (2000).

[64] J. Doerfoert, E. Träbert, and A. Wolf, *Hyperfine Interactions 99,* 155 (1996).

[65] A. J. Smith, P. Beiersdorfer, K. J. Reed, A. L. Osterheld, V. Decaux, K. Widman, and M. H. Chen, *Phys. Rev. A 62* (2000) 012704.

[66] D. P. Moehs and D. A. Church, *Astrophys. J. Lett. 516,* L111 (1999).

[67] K. M. Aggarwal, A. Hibbert, and F. P. Keenan, *Astrophys. J. Suppl. Ser. 108,* 393 (1997).

[68] S. S. Tayal, *J. Phys. B 32,* 5311 (1999); *Atom. Data Nucl. Data Tables 67,* 331 (1997).

[69] N. C. Deb and S. S. Tayal, *Atom. Data Nucl. Data Tables 69,* 161 (1998).

[70] S. N. Nahar, *Atom. Data Nucl. Data Tables 72,* 129 (1999).

[71] A. K. Pradhan, *Phys. Script. T83,* 69 (1999).

[72] N. C. Deb, K. M. Aggarwal, and A. Z. Msezane, *Astrophys. J. Suppl. Ser. 121,* 265 (1999).

[73] K. M. Aggarwal, P. H. Norrington, K. L. Bell, F. P. Keenan, G. J. Pert, and S. J. Rose, *Atom. Data Nucl. Data Tables 74,* 157 (2000).

[74] M. van Noort, T. Lanz, H. J. G. L. M. Lamers, R. L. Kurucz, R. Ferlet, G. Hébrard, and A. Vidal-Madjar, *Astron. Astrophys. 334,* 633 (1998); R. L. Kurucz, *Phys. Scripta T47,* 110 (1993).

[75] J.-U. Ness, R. Mewe, J. H. M. M. Schmitt, A. J. J. Raassen, D. Porquet, J. S. Kaastra, R. L. J. van der Meer, V. Burwitz, and P. Oredehl, *Astron. Astrophys. 367*, 282 (2001).

[76] S. M. Kahn, M. A. Leutenegger, J. Cottam, G. Rauw, J.-M. Vreux, A. J. F. den Boggende, R. Mewe, and M. Güdel, *Astron. Astrophys. 365*, L312 (2001).

[77] A. K. Pradhan, D. W. Norcross, and D. G. Hummer, *Astrophys. J. 246,* 1031 (1981).

[78] C. M. Lisse and 11 co-authors, *Science 274*, 205 (1996).

[79] C. M. Lisse, D. J. Christian, K. Dennerl, K. J. Meech, R. Petre, H. A. Weaver, and S. J. Wolk, *Science* (in press, 2001).

[80] M. J. Mumma, V. A. Krasnopolsky, and M. J. Abbott, *Astrophys. J. 491,* L125 (1997).

[81] V. A. Krasnopolsky, M. J. Mumma, and M. J.Abbott, *Icarus 146*, 152 (2000); V. A. Krasnopolsky, *J. Geophys. Res. 103,* 2069 (1998).

[82] V. A. Krasnopolsky, M. J. Mumma, M. J. Abbott, B. C. Flynn, K. J. Meech, D. K. Yeomans, P. D. Feldman, and C. B. Cosmovici, Sc*ience 277*, 1488 (1997).

[83] R. M. Häberli, T. I. Gombosi, D. L. De Zeeuw, M. R. Combi, and K. G. Powell, *Science 276,* 939 (1997).

[84] A. Owens and 9 co-authors, *Nucl. Phys. B 69/1-3,* 735 (1998).

[85] K. Dennerl , J. Engelhauser, and J. Trumper, *Science 277*, 1625 (1997).

[86] T. E. Cravens, *Adv. Space Res. 26*, 1443 (2000).

[87] B. J. Wargelin and J. J. Drake, *Astrophys. J. 546*, L57 (2001).

[88] T. E. Cravens, *Astrophys. J. 532,* L153 (2000).

[89] T. G. Northrop, C. M. Lisse, M. J. Mumma, and M. D. Desch, *Icarus 127*, 246 (1997).

[90] V. A. Krasnopolsky, *J. Geophys. Res. 103*, 2069 (1998).

[91] T. E. Cravens, *Geophys. Res. Letters 24*, 105 (1997).

[92] T. I. Gombosi, D. De Zeeuw, R. M. Häberli, and K. G. Powell, *J. Geophys. Res. 101*, 15 233 (1996).

[93] C. M. Lisse, C. M. *et al.*, *Earth, Moon and Planets 77*, 283 (1999).

[94] V. Kharchenko and A. Dalgarno, *J. Geophys. Res. 105*, 18 351 (2000).

[95] N. A. Schwadron and T. E. Cravens, *Astrophys. J. 544*, 558 (2000).

[96] R. Wegmann, H. U. Schmidt, C. M. Lisse, K. Dennerl, and J. Englhauser, *Planet. Space Sci. 46*, 603 (1998).

[97] H. Ryufuku, K. Sasaki, and T. Watanabe, P*hys. Rev. A 21*, 745 (1980).

[98] J. B. Greenwood, I. D.Williams, S. J. Smith, and A. Chutjian, *Phys. Rev. A 63, 062707* (2001).

[99] J. B. Greenwood, I. D.Williams, S. J. Smith, and A. Chutjian, *Astrophys. J. Lett. 533,* L175 (2000).

[100] J. B. Greenwood, I. D. Williams, S. J. Smith, and A. Chutjian, in *Applications of Accelerators in Research and Industry* (ed. J. L. Duggan and I. L. Morgan, CP576, AIP, New York, 2001) p. 157

[101] J. B. Greenwood, I. D. Williams, S. J. Smith, and A. Chutjian, *Phys. Scripta T1B*, 0000 (2001) (in press).

Table 1. Highly-charged heavy ions present in the solar wind, and their abundance relative to the total oxygen-ion abundance (taken as unity). Abundances in the slow (~400 km s^{-1}) and fast (~750 km s^{-1}) solar-wind distributions are listed, as well as total ion energies in each (adapted from Ref. [95]).

HCI, X^{q+}	$[X^{q+}]/[O]$ fast	$[X^{q+}]/[O]$ slow	Energy (keV) fast	slow
C^{6+}	0.085	0.318	35.0	9.95
C^{5+}	0.440	0.210		
N^{7+}	0.000	0.006	40.8	11.6
N^{6+}	0.011	0.058		
N^{5+}	0.127	0.065		
O^{8+}	0.000	0.070	46.6	13.3
O^{7+}	0.030	0.200		
O^{6+}	0.970	0.730		
Ne^{8+}	0.102	0.084	58.3	16.6
Ne^{7+}	0.005	0.004		
Mg^{10+}	0.029	0.098	70.0	19.9
Mg^{9+}	0.044	0.052		
Mg^{8+}	0.028	0.041		
Mg^{7+}	0.007	0.017		
Mg^{6+}	0.003	0.009		
Si^{10+}	0.024	0.021	81.6	23.2
Si^{9+}	0.045	0.049		
Si^{8+}	0.022	0.057		
Si^{7+}	0.002	0.000		
S^{11+}	0.001	0.000	93.3	26.5
S^{10+}	0.008	0.005		
S^{9+}	0.027	0.016		
S^{8+}	0.023	0.019		
S^{7+}	0.005	0.006		

S^{6+}	0.001	0.002		
Fe^{13+}	0.005	0.002	163	46.4
Fe^{12+}	0.017	0.007		
Fe^{11+}	0.025	0.023		
Fe^{10+}	0.025	0.031		
Fe^{9+}	0.015	0.041		
Fe^{8+}	0.005	0.034		
Fe^{7+}	0.001	0.007		

Table 2. Compendium of home pages for satellite operations, and of several atomic databases.

Satellite	Home Page
Hubble Space Telescope	http://www.stsci.edu/
SOHO	http://sohowww.nascom.nasa.gov/
FUSE	http://fuse.pha.jhu.edu/
EUVE (mission discontinued)	http://archive.stsci.edu/euve/simple_euve.html
ROSAT	http://wave.xray.mpe.mpg.de/rosat
TRACE	http://vestige.lmsal.com/TRACE
Chandra X-Ray Observatory	http://asc.harvard.edu/
Constellation X-Ray Mission	http://constellation.gsfc.nasa.gov/
XMM-*Newton*	http://xmm.vilspa.esa.es/
SOFIA	http://sofia.arc.nasa.gov/
Infrared Space Observatory	http://www.iso.vilspa.esa.es/

Atomic Database	Home Page
CHIANTI	http://wwwsolar.nrl.navy.mil/chianti.html
NIST Atomic Database	http://physics.nist.gov/cgi-bin/AtData/levels_form
Atomic Data for Astrophysics	http://www.pa.uky.edu/~verner/atom.html
The IRON Project	http://www.am.qub.ac.uk/projects/iron/
comet-related collision research	http://www.qub.ac.uk/mp/ampr/networks/cometxrays.htm

Figure Captions

Figure 1. Theoretical Fe XXI line emission ratios $R_1 = I(2s^2 2p^2\ ^3P_1 - 2s2p^3\ ^5S) / I(2s^2 2p^2\ ^3P_0 - 2s^2 2p^2\ ^3P_1)$ (top), and $R_2 = I(2s^2 2p^2\ ^3P_1 - 2s^2 2p^2\ ^1S) / I(2s^2 2p^2\ ^3P_0 - 2s^2 2p^2\ ^3P_1$ (bottom) in a 15-state ***R***-matrix calculation [12]. Stars are results in a distorted-wave calculation of Ref. [15]. The ratios make suitable diagnostics of N_e in the region above about $N_e \approx 10^{11}$ cm^{-3}, a density encountered in strong solar and stellar flares.

Figure 2. Experimental results (filled circles) and results of a 27-state ***R***-matrix theory (solid line) for the $^3P \rightarrow {}^5S^o$ transition in S^{2+} [29]. The theoretical results have been convoluted with an experimental, CM-variable Gaussian electron-energy width. The dashed line through the experimental data is meant to guide the eye.

Figure 3. Coupling of database information (*CHIANTI*) with satellite observations (*EUVE*) to model the emissions from the dwarf nova *OY Carinae* in a superoutburst mode [57]. Emitting species are indicated at the top. The observed spectrogram is shown as gray, dotted histogram; the net model spectrum by the thick solid line, and the individual ion contributions by the thin solid line. The O VI model spectrum is the shaded area, and carets indicate nonresonance O VI lines.

Figure 4. Spectra (dot-dash line), fit (solid line), and background (dotted line) for the resonance (*r*), intercombination (*i*), and forbidden (*f*) transitions in the He-like C V, N VI, and O VII triplets. Observations were made at the star *Capella* using the LETGS aboard *Chandra* [75].

Figure 5. Charge-exchange, X-ray photon count rate per cometary neutral, for the condition of fast solar wind and optically thin target. The contributing solar-wind species are listed at the right. A flat cross section *vs* energy is assumed, and multiple charge-exchanges ($\Delta q \geq 2$) are neglected (from Ref. [94]).

Figure 6. X-ray spectra for collisions of O^{8+} in He, H_2, CO_2, and H_2O at a total ion energy of 56 keV. Underlying curves are the Lyman contributions $np \rightarrow 1s$, and dashed line is the X-ray detector response curve [101].

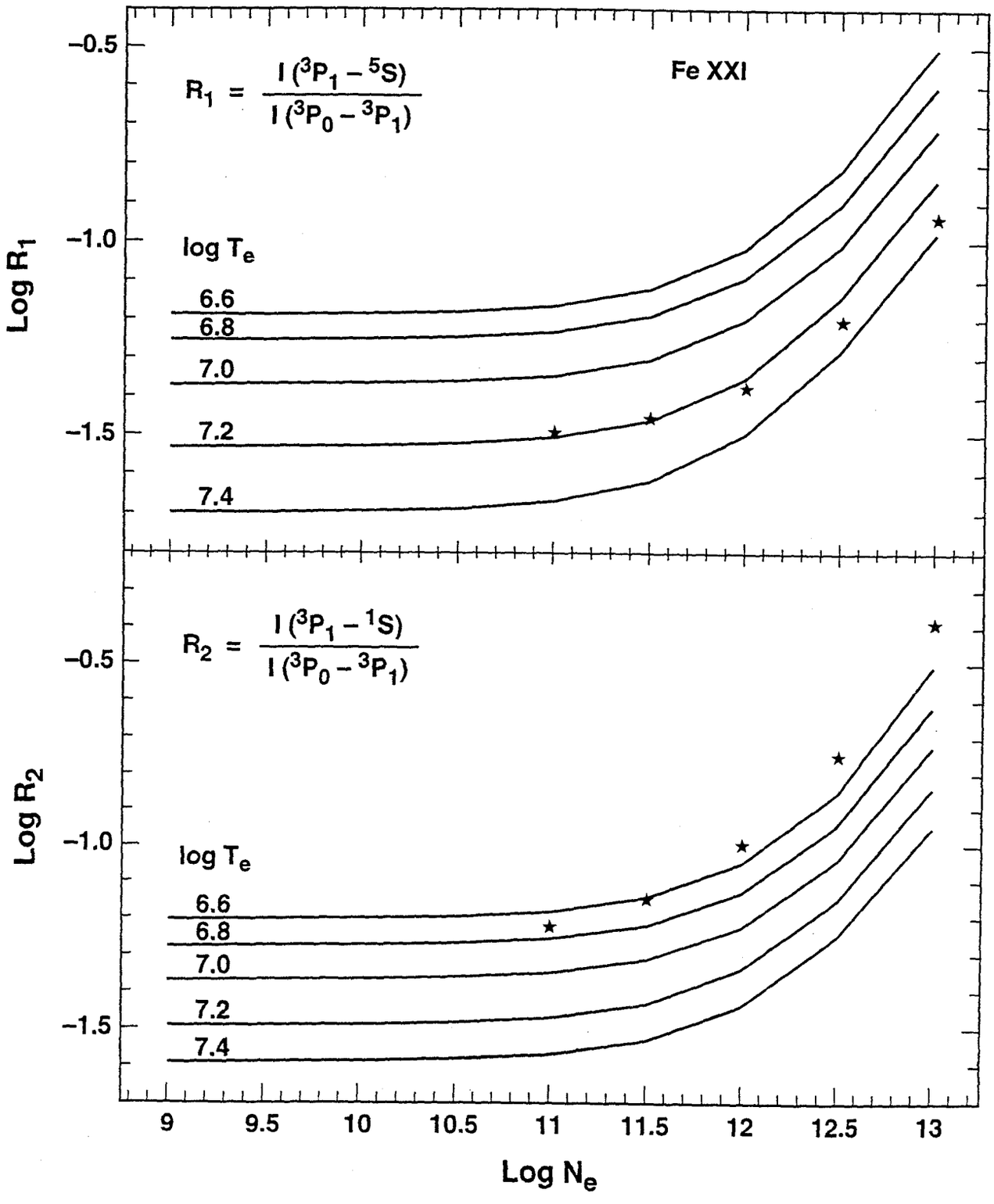
Fe XXI
$R_1 = \frac{I(^3P_1 - ^5S)}{I(^3P_0 - ^3P_1)}$
log T_e
6.6
6.8
7.0
7.2
7.4
Log R_1
−0.5
−1.0
−1.5
$R_2 = \frac{I(^3P_1 - ^1S)}{I(^3P_0 - ^3P_1)}$
log T_e
6.6
6.8
7.0
7.2
7.4
Log R_2
−0.5
−1.0
−1.5
9
9.5
10
10.5
11
11.5
12
12.5
13
Log N_e

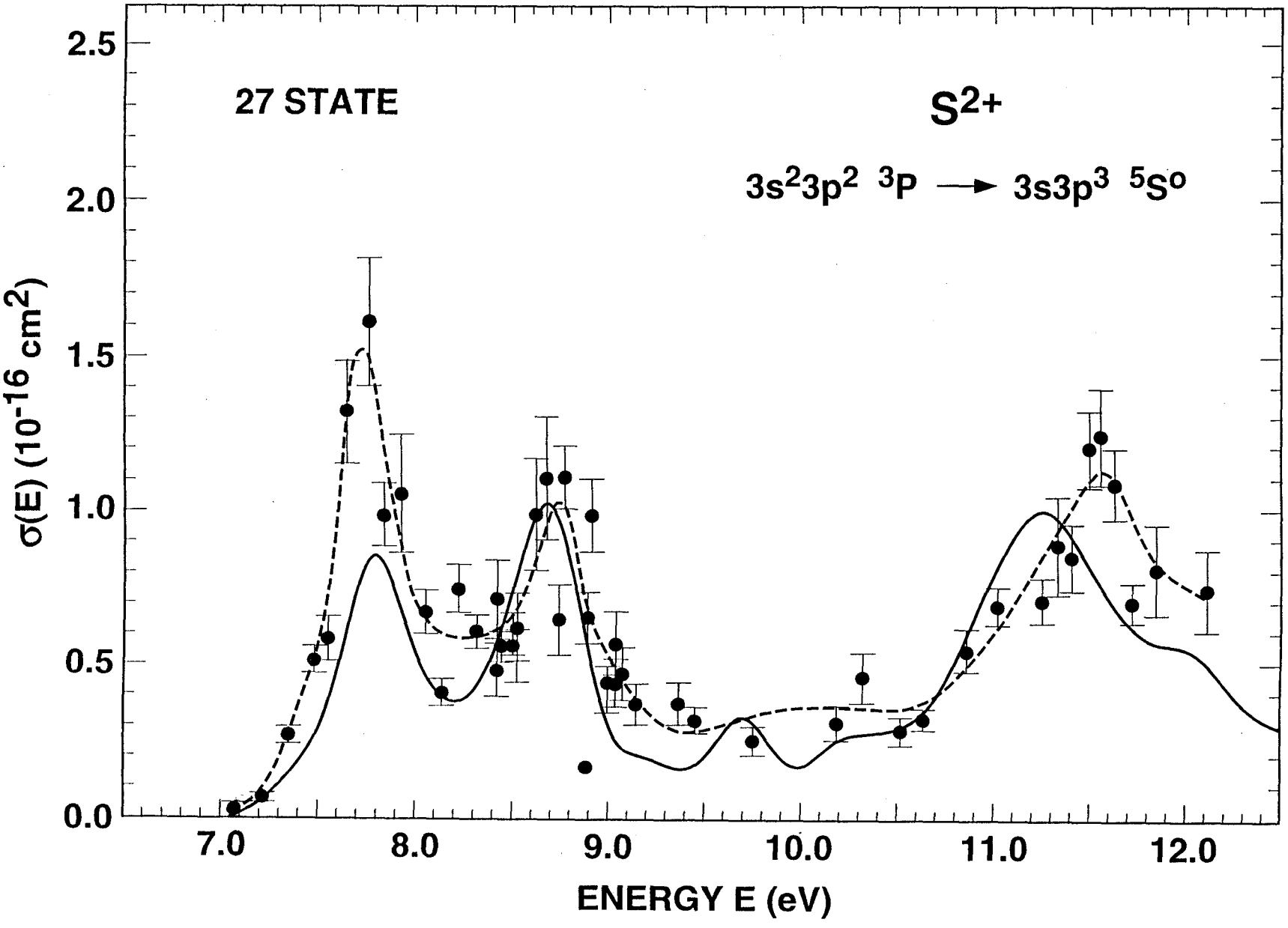
27 STATE
S2+
3s23p2 3P → 3s3p3 5So
σ(E) (10-16 cm2)
2.5
2.0
1.5
1.0
0.5
0.0
7.0
8.0
9.0
10.0
11.0
12.0
ENERGY E (eV)

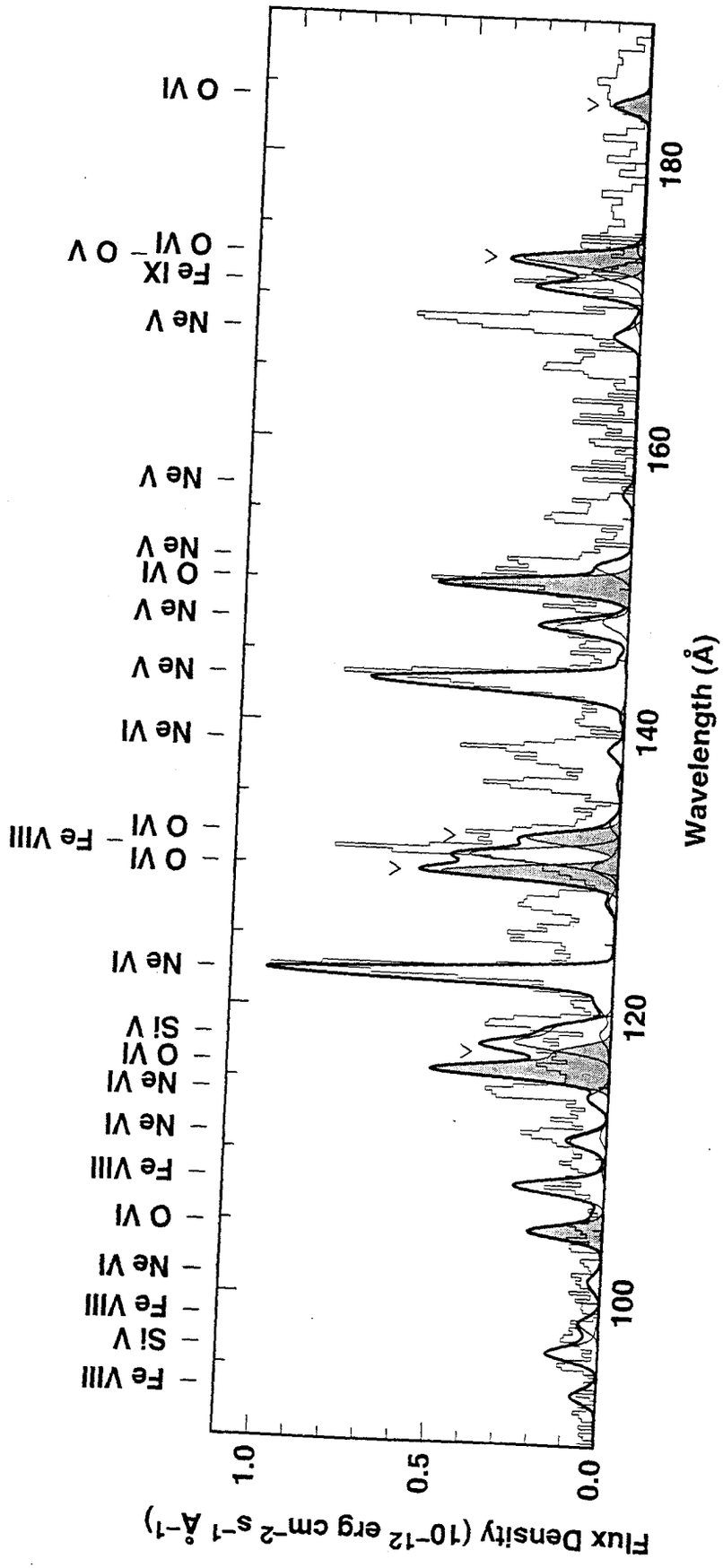
Flux Density (10^{-12} erg cm^{-2} s^{-1} Å^{-1})
1.0
0.5
0.0
100
120
140
160
180
Wavelength (Å)
Fe VIII
Si V
Fe VIII
Ne VI
O VI
Fe VIII
Ne VI
Ne VI
O VI
Si V
Ne VI
Ne VI
O VI
O VI
Fe VIII
Ne VI
Ne V
Ne V
O VI
Ne V
Ne V
Ne V
Fe IX
O VI
O V
O VI

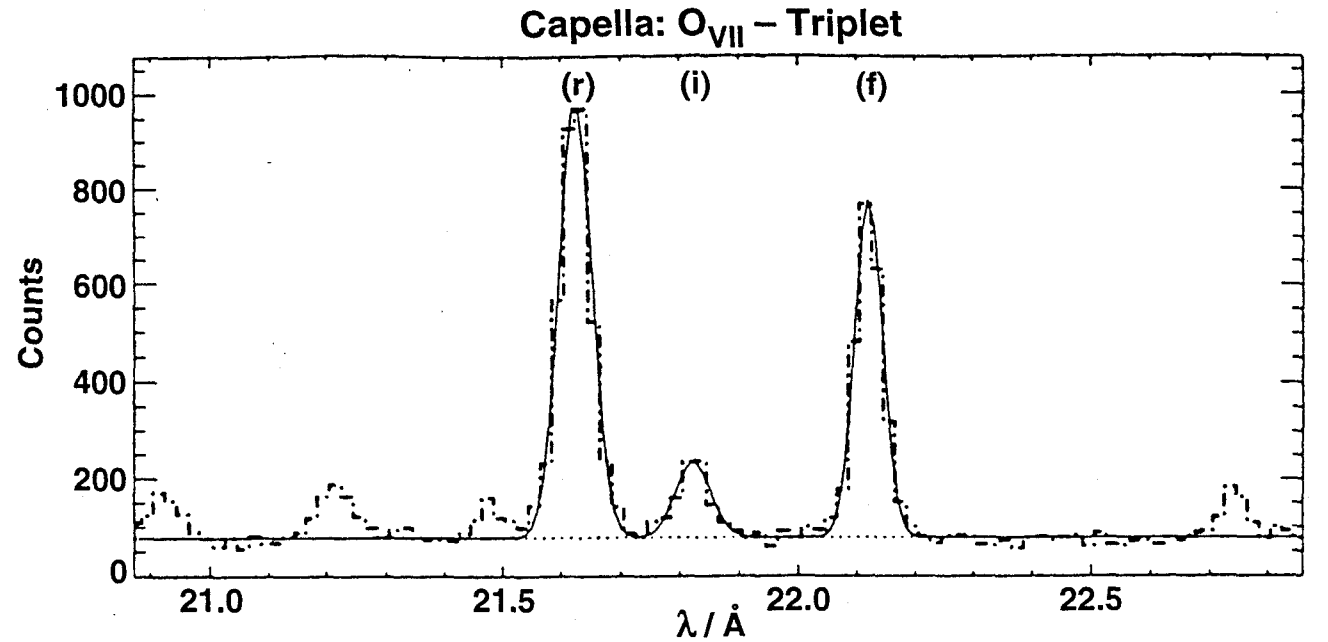
Capella: O_{VII} – Triplet
(r)
(i)
(f)
Counts
λ / Å

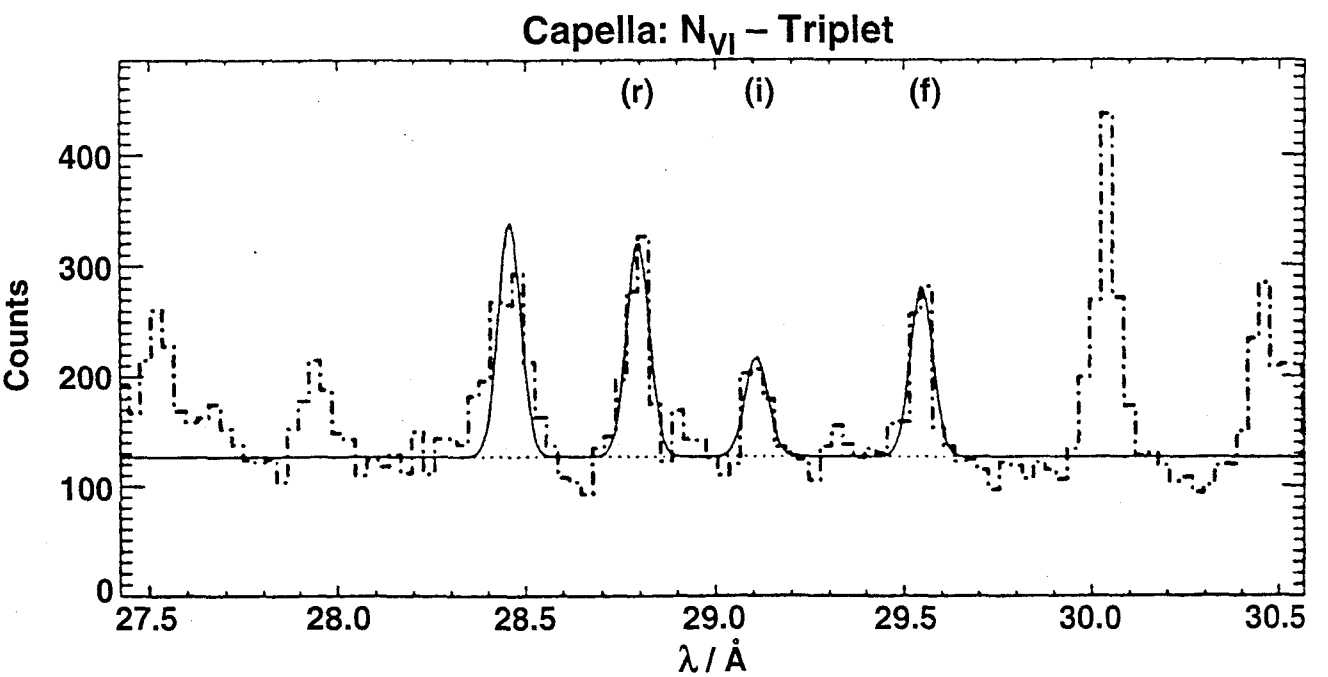
Capella: N_{VI} – Triplet
(r)
(i)
(f)
Counts
λ / Å

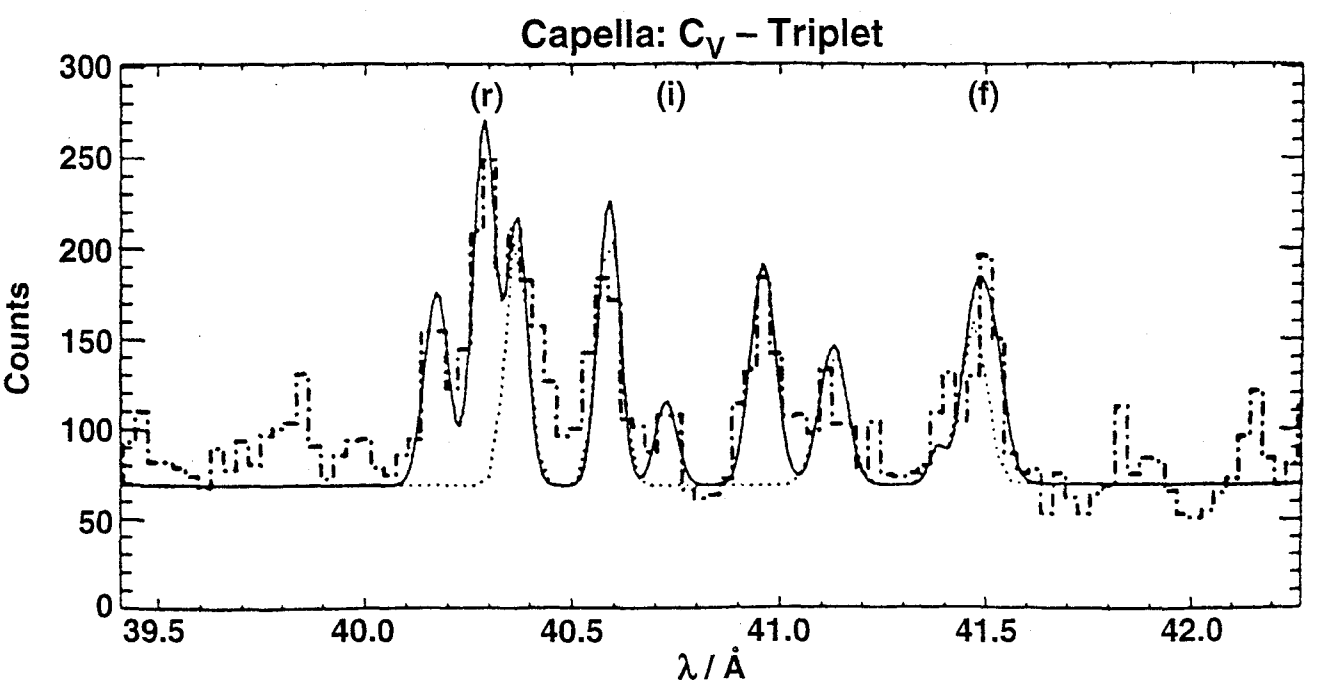
Capella: C_V – Triplet
(r)
(i)
(f)
Counts
λ / Å

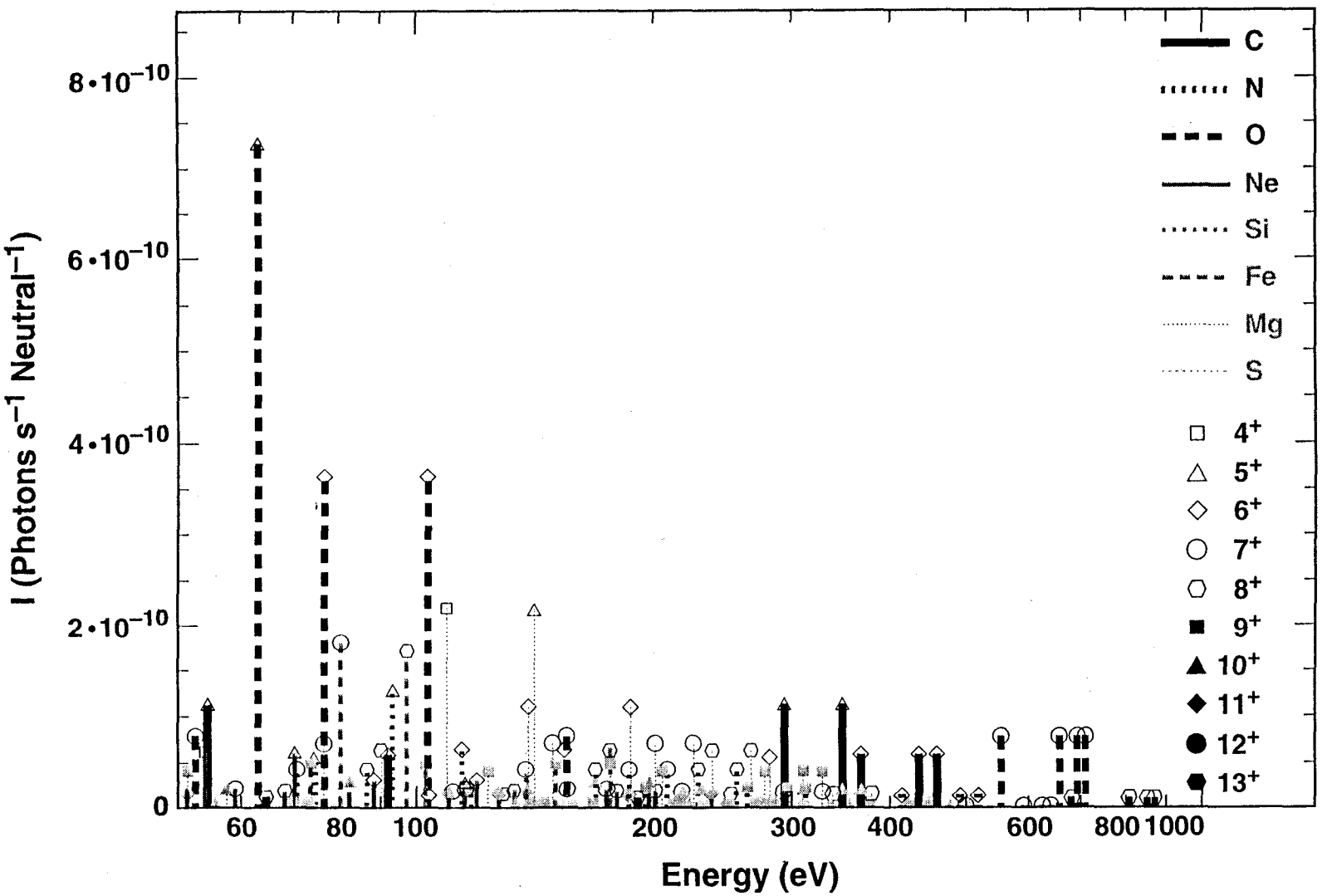
I (Photons s^{-1} Neutral^{-1})
8•10^{-10}
6•10^{-10}
4•10^{-10}
2•10^{-10}
0
60
80
100
200
300
400
600
800
1000
Energy (eV)
C
N
O
Ne
Si
Fe
Mg
S
4^{+}
5^{+}
6^{+}
7^{+}
8^{+}
9^{+}
10^{+}
11^{+}
12^{+}
13^{+}

5

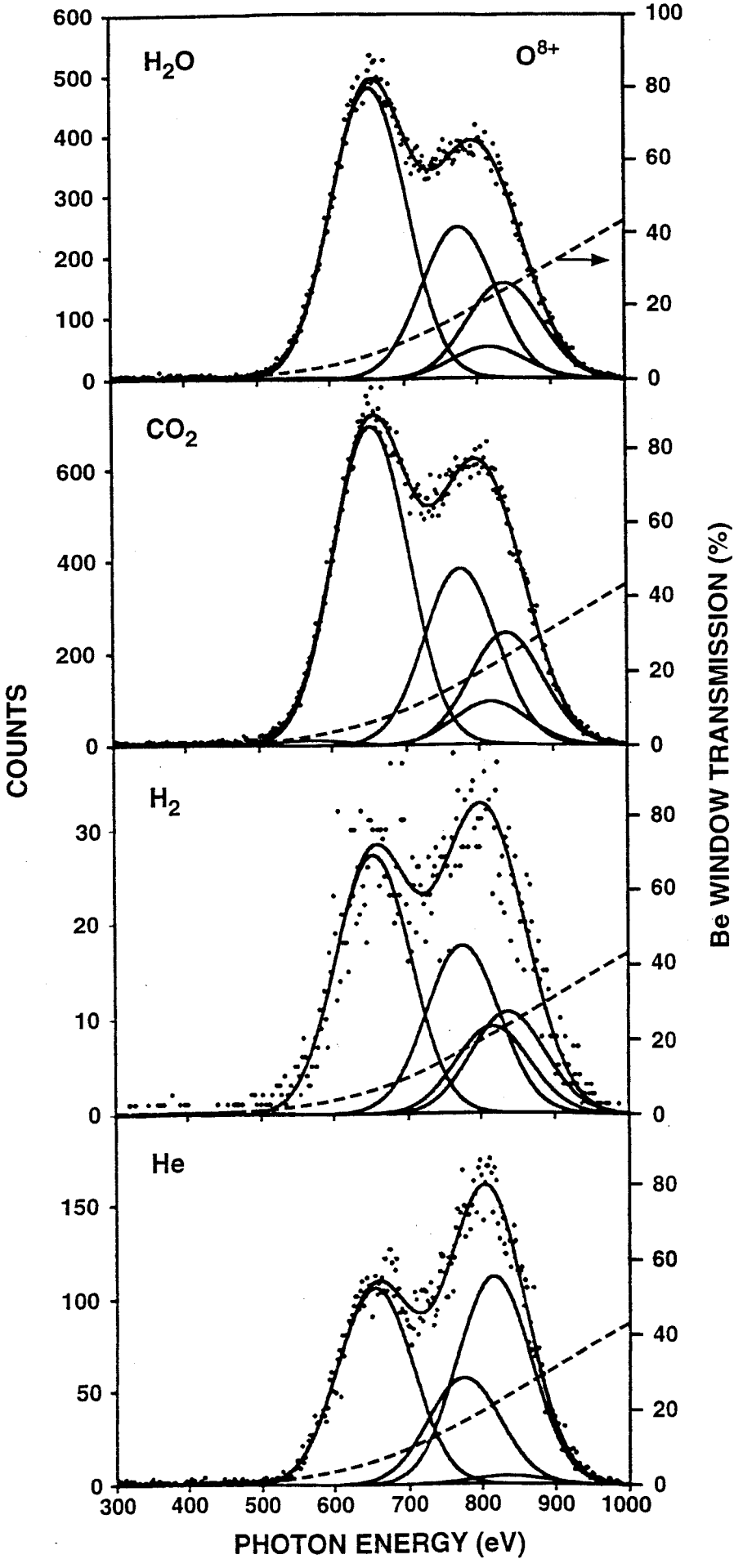
H2O
O8+
CO2
H2
He
COUNTS
Be WINDOW TRANSMISSION (%)
PHOTON ENERGY (eV)
300
400
500
600
700
800
900
1000